Article

Current Biology

Obstacle avoidance in aerial pursuit

Highlights

- Harris' hawks chasing targets make one-off steering corrections to avoid obstacles
- At a threshold range, they aim for a point one wing length from an obstacle's edge
- This discrete open-loop correction modifies their continuous closed-loop pursuit
- Hawks can thereby avoid obstacles while remaining locked-on to their target

Authors

Caroline H. Brighton, James A. Kempton, Lydia A. France, Marco KleinHeerenbrink, Sofía Miñano, Graham K. Taylor

Correspondence

graham.taylor@biology.ox.ac.uk

In brief

Brighton et al. use high-speed motion capture to analyze how hawks resolve the conflict between prey pursuit and obstacle avoidance when hunting in clutter. Obstructed pursuit is well modeled by a biased guidance law that combines closed-loop feedback on target motion with an open-loop steering correction at some threshold distance to an obstacle.

Brighton et al., 2023, Current Biology *33*, 3192–3202
August 7, 2023
https://doi.org/10.1016/j.cub.2023.06.047

CellPress

CellPress
OPEN ACCESS

Current Biology

Article

Obstacle avoidance in aerial pursuit

Caroline H. Brighton,[1] James A. Kempton,[1] Lydia A. France,[1,2] Marco KleinHeerenbrink,[1] Sofía Miñano,[1,3] and Graham K. Taylor[1,4,*]
[1]Department of Biology, University of Oxford, OX1 3SZ Oxford, UK
[2]The Alan Turing Institute, NW1 2DB London, UK
[3]Advanced Research Computing Centre, University College London, WC1E 6BT London, UK
[4]Lead contact
*Correspondence: graham.taylor@biology.ox.ac.uk
https://doi.org/10.1016/j.cub.2023.06.047

SUMMARY

Pursuing prey through clutter is a complex and risky activity requiring integration of guidance subsystems for obstacle avoidance and target pursuit. The unobstructed pursuit trajectories of Harris' hawks *Parabuteo unicinctus* are well modeled by a mixed guidance law feeding back target deviation angle and line-of-sight rate. Here we ask how their pursuit behavior is modified in response to obstacles, using high-speed motion capture to reconstruct flight trajectories recorded during obstructed pursuit of maneuvering targets. We find that Harris' hawks use the same mixed guidance law during obstructed pursuit but appear to superpose a discrete bias command that resets their flight direction to aim at a clearance of approximately one wing length from an upcoming obstacle as they reach some threshold distance from it. Combining a feedback command in response to target motion with a feedforward command in response to upcoming obstacles provides an effective means of prioritizing obstacle avoidance while remaining locked-on to a target. We therefore anticipate that a similar mechanism may be used in terrestrial and aquatic pursuit. The same biased guidance law could also be used for obstacle avoidance in drones designed to intercept other drones in clutter, or to navigate between fixed waypoints in urban environments.

INTRODUCTION

Collision avoidance[1–4] and target pursuit[5–8] are challenging flight behaviors for any animal or autonomous vehicle, but their interaction is even more so.[9–11] For predators adapted to hunting in clutter, the demands of these two tasks will often come into conflict,[12] requiring effective reconciliation to avoid loss of the target or a hazardous collision. Technical approaches to autonomous obstacle avoidance commonly combine active mapping[13] and path planning[14] algorithms, but these approaches are computationally costly[15] and are unlikely to be effective during closed-loop pursuit of a target maneuvering through clutter. Consequently, collision avoidance must instead be implemented reactively during prey pursuit. For instance, the combined pursuit-avoidance behavior of predatory flies has been modeled successfully using visual feedback on target motion and obstacle looming,[16] although it is unclear how well the proposed behavioral algorithm will generalize to complex environments with many obstacles. Reactive behavioral dynamics[17] have also been observed in humans walking around obstacles to reach a stationary goal[18] or moving target,[19] inspiring algorithmic implementations in autonomous systems.[20,21] Obstacle avoidance has been studied in echolocating bats catching stationary targets,[12] and there have been several neuromorphic implementations of sonar obstacle avoidance in robots targeting fixed goals.[22,23] Nevertheless, it remains unknown how aerial predators reconcile the conflict between obstacle avoidance and target pursuit in clutter, and this remains an open problem in robotics.

The unobstructed pursuit behavior of Harris' hawks *Parabuteo unicinctus* has been well characterized,[11] but their natural mode of hunting involves short flights targeting terrestrial prey in habitat clutter.[24] Here, we use a high-speed motion capture system to reconstruct the flight trajectories of N = 4 Harris' hawks chasing a lure towed along an unpredictable path about a series of pulleys in a large hall with or without obstacles (Video S1). We used two rows of hanging ropes as obstacles: the first row forming a dense clump that the bird had to fly around, and the second simulating a row of trees that the bird had to fly between (Figures 1A and 1B). We then simulated these data computationally using several alternative models of the guidance dynamics. We find that the hawks' obstructed pursuit trajectories are well modeled by the same mixed guidance law used during obstructed pursuit (Equation 1), but with the superposition of a discrete bias command that resets their flight direction to aim at a clearance of approximately one wing length from an upcoming obstacle as they reach some threshold distance from it. This biased guidance law provides an effective means of prioritizing obstacle avoidance while remaining locked-on to the target. We conclude by discussing possible applications of this mechanism to autonomous systems.

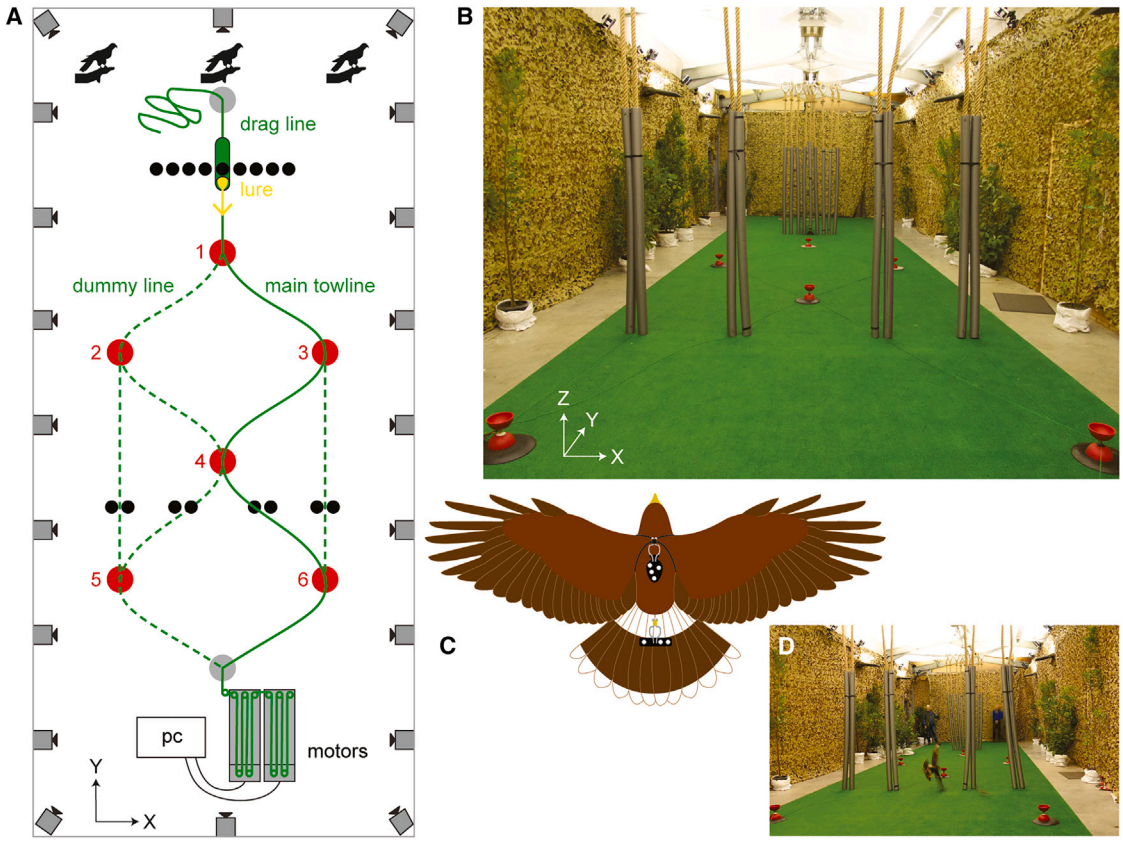

Figure 1. Overview of experimental setup

(A) Overhead view of flight hall. Each of the N = 4 Harris' hawks flew from one of three alternative starting positions (bird icons), chasing a food lure (yellow arrow) that was pulled forward by a pair of linear motors (gray rectangles) from its starting position on a towline with a trailing drag line (green solid line) that ran around 3 or 4 out of 6 pulleys (red circles). Dummy towlines (green dashed lines) were laid around the remaining pulleys, so that the bird would not be able to anticipate which of the 6 alternative paths the lure would follow. The hawk and lure were tracked by 20 motion capture cameras positioned around the room (camera icons). Ropes (black circles) were hung as obstacles in the configuration shown for the test flights with obstacles.

(B) Photo of experimental set-up looking from the linear motors back toward the starting positions of the bird and lure; note the diffuse overhead lighting provided by bouncing light from the 8 LED up-lights positioned around the walls. Shrubs and trees were placed down the sides of the room to provide visual contrast and discourage flight outside of the central test area.

(C) Overhead view of Harris' hawk, showing the marker templates worn on the back and tail (black patches) together with the attached retroreflective markers (white circles).

(D) Still frame from Video S1, showing typical pursuit behavior by first-year male Rhaegal.

See also Video S1.

RESULTS

Our dataset comprises four distinct subsets: (1) a set of n = 128 obstacle-free training flights collected over an initial 8 days, (2) a set of n = 16 obstacle familiarization flights collected the following day, then (3) a set of n = 103 obstacle-free test flights, and (4) a set of n = 154 obstacle test flights, where (3) and (4) were collected over 15 days on which the presence or absence of obstacles was randomized (STAR Methods). The sampling of these subsets was approximately balanced across the N = 4 individuals (Table S1).

Model validation

Previous work[11] has found that the unobstructed pursuit trajectories of Harris' hawks are well modeled by assuming their turning is commanded at an angular velocity:

$$\dot{\gamma}(t) = N\dot{\lambda}(t-\tau) - K\delta(t-\tau), \qquad \text{(Equation 1)}$$

where N, K, and τ are fitted constants; $\dot{\lambda}$ is the angular rate of the line of sight from the pursuer to the target; δ is the signed deviation angle between the pursuer's flight direction and its line of sight to the target; and t is time. Because Equation 1 mixes feedback on the line-of-sight rate $\dot{\lambda}$ and the target deviation angle δ, it is described as a mixed guidance law. We begin by using the n = 128 obstacle-free training flights to validate Equation 1 at the previously published parameter settings[11] of $N = 0.7$, $K = 1.2\ s^{-1}$, and $\tau = 0.09$ s. We match the hawk's simulated flight speed to its measured flight speed and use Equation 1 to model its horizontal turning behavior, taking the measured trajectory of the lure as a given (but see Paul and Ghose[25] for an analytical model of speed variation fitted to the earlier data from Brighton and Taylor[11]). We match the initial conditions of each simulation

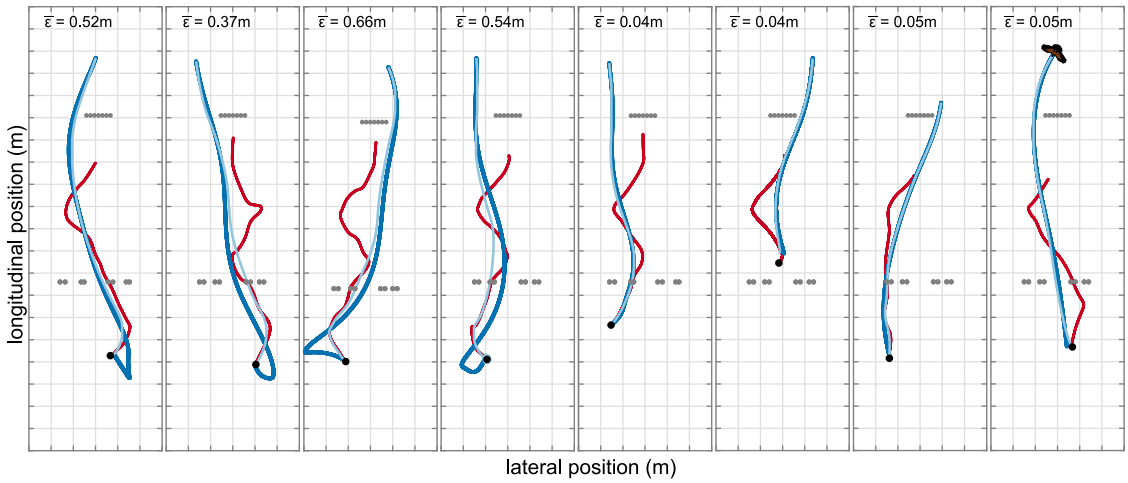

Figure 2. Measured pursuit trajectories of Harris' hawks compared to guidance simulations under the mixed guidance law

Each panel represents a single obstacle test flight and plots the hawk's measured flight trajectory (dark blue) in pursuit of the lure (dark red) up to the point of capture (black dot). The measured data are compared to a simulation of the hawk's trajectory (light blue) under the refined mixed guidance law (Equation 1) with best-fitting parameters $N = 0.75$, $K = 1.25\ s^{-1}$, and $\tau = 0.01$ s fitted to the union of the test flights with and without obstacles. The displayed values of $\bar{\varepsilon}$ show the mean prediction error for each simulation. The lefthand panels show the four longest obstacle test flights; the righthand panels show the four obstacle test flights with the lowest mean prediction error relative to the total distance flown, for flights >9 m in length. Grid spacing: 1 m. See also Figure S1.

to the measured data. We define the instantaneous prediction error of the simulation, $\varepsilon(t)$, as the distance between the bird's measured and simulated position, which we summarize by reporting the mean prediction error ($\bar{\varepsilon}$) for each flight, and its median ($\tilde{\varepsilon}$) over all the flights within each subset.

The resulting simulations typically had a low mean prediction error, with a median value of $\tilde{\varepsilon} = 0.22$ m over the n = 128 flights (95% CI: 0.20, 0.28 m). By comparison, the median over the independent dataset of n = 50 obstacle-free flights to which Equation 1 was originally fitted was $\tilde{\varepsilon} = 0.34$ m (95% CI: 0.24, 0.53 m). Equation 1 therefore models our sample of n = 128 obstacle-free training flights at least as well as the sample of n = 50 outdoor flights to which it was fitted, validating its suitability as a model of unobstructed pursuit behavior in Harris' hawks. Because Equation 1 feeds back the deviation angle δ in addition to the line-of-sight rate $\dot{\lambda}$, it produces a characteristic tail-chasing behavior, which is expected to produce implicit collision avoidance if the pursuer is chasing a target that is itself weaving between obstacles. The lure traveled through the gaps between obstacles on the n = 16 obstacle familiarization flights, so we tested this prediction by using Equation 1 to simulate these flights at the published parameter settings.[11] Although the model does not always predict the hawk's turning behavior closely at the point of capture, it predicts earlier sections of each flight well, following the lure through the gaps between obstacles (Figure S1A). The target pursuit subsystem that Equation 1 describes is therefore capable of producing a safe path through clutter when chasing a target that itself passes safely between obstacles.

Model refinement

We next refined the parameters of the mixed guidance law (Equation 1) in relation to the n = 257 test flights that we recorded. For direct comparability with the results of our modeling using the original mixed guidance law,[11] all of our simulations begin from 0.09 s after the start of each recording, allowing for a sensorimotor delay of $\tau \leq 0.09$ s. We began by fitting separate models to the test flights with and without obstacles, finding the guidance parameter settings that minimized the median of the mean prediction error, $\tilde{\varepsilon}$, over each subset of flights (STAR Methods). However, as the optimized parameters were similar for each subset ($N = 0.75$, $K = 1.15\ s^{-1}$, and $\tau = 0.005$ s for the n = 103 obstacle-free test flights; $N = 0.75$, $K = 1.15\ s^{-1}$, and $\tau = 0.015$ s for the n = 154 obstacle test flights) and were close to those fitted in previous work,[11] we re-fitted the model to the union of the test flights with and without obstacles (Figure 2; see also Figure S1B).

Because flights with obstacles are overrepresented in this sample relative to flights without obstacles, we used a subsampling procedure in which we randomly subsampled 80 flights without replacement from each subset and identified the parameter settings that minimized $\tilde{\varepsilon}$ over that subsample (STAR Methods). We repeated this sampling experiment 100,000 times and took the median of the best-fitting parameter settings as our refined model. The goodness of fit of this model with refined parameter settings of $N = 0.75$, $K = 1.25\ s^{-1}$, and $\tau = 0.010$ s was similar for both the n = 103 obstacle-free test flights ($\tilde{\varepsilon} = 0.14$ m; 95% CI: 0.12, 0.19 m; Figure S1B) and the n = 154 obstacle test flights ($\tilde{\varepsilon} = 0.16$ m; 95% CI: 0.14, 0.21 m; Figure 2). Moreover, it performed marginally better on the validation data from the n = 128 obstacle-free training flights ($\tilde{\varepsilon} = 0.21$ m; 95% CI: 0.17, 0.26 m) than the original version of the mixed guidance law.[11] We therefore take the refined mixed guidance law as our best-supported model of the target pursuit subsystem of Harris' hawks.

Take-off direction is biased to avoid obstacles

The refined mixed guidance law usually predicted a collision-free path around the first row of obstacles (Figure 2), which reflects the fact that our simulations were initialized using the bird's

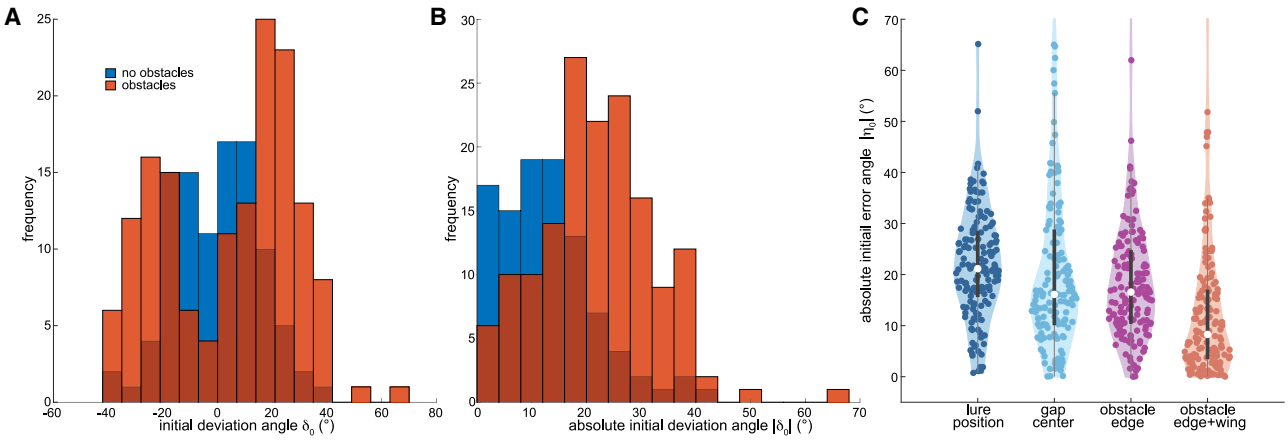

Figure 3. Bias in take-off direction with respect to lure

(A) Histogram of the initial deviation angle, δ_0, defined as the angle between the hawk's flight direction and its line of sight to the lure, sampled at the time $t = 0$ from which the guidance simulations began.

(B) Histogram of the absolute initial deviation angle, $|\delta_0|$.

(C) Violin plots of the absolute initial error angle, $|\eta_0|$, defined as the angle between the hawk's initial flight direction and its initial line of sight to the target stated beneath each plot. In the special case that the target is the lure (denoted lure "position"), then $|\eta_0| \equiv |\delta_0|$. The three alternative target definitions include (1) the nearest edge of the first obstacle (denoted "obstacle edge"), (2) the center of the gap between this and the wall (denoted "gap center"), and (3) an intermediate position approximately one wing length (0.5 m) into the gap from the edge of the obstacle (denoted "obstacle edge + wing"). Data are shown for all n = 154 obstacle test flights and for n = 103 obstacle-free test flights, having dropped all 3 flights on which the hawk had already traveled beyond the location of the first obstacle by the point at which the guidance simulations began. Each violin plot displays a kernel density estimate of the data overlain with the actual data points; the thick black line in the center of of each plot extends between the lower and upper quartiles; a thin vertical line displays the range of the data points not considered outliers; the median is shown as a white dot.

measured take-off velocity. Hence, if the hawk set its take-off direction to avoid the first set of obstacles, then the resulting bias in the initial value of its deviation angle δ would be embedded in its subsequent pursuit behavior. We tested this by comparing the distribution of the initial deviation angle, δ_0, measured between the hawk's flight velocity and its line of sight to the lure at the start of the simulation, for the different test flight subsets.

Whereas the distribution of δ_0 was unimodal with a mode at $\delta_0 \approx 0$ for the test flights without obstacles, it was bimodal with modes at $\delta_0 \approx \pm 20^\circ$ for the test flights with obstacles (Figure 3A). Accordingly, the median absolute initial deviation angle (Figure 3B) was larger for the test flights with obstacles (21.2°; 95% CI: 19.8°, 23.8°; n = 154 flights) than for those without (11.7°; 95% CI: 9.1°, 13.9°; n = 103 flights; see Figure 3 legend for exclusions). Hence, whereas the hawks took off toward the lure when there were no obstacles present, they biased their take-off away from any obstacle that was blocking their path to the lure.

We next tested whether this observed bias in take-off direction was necessary and sufficient to ensure that the hawk's target pursuit subsystem would produce a safe path around the first obstacle. We checked this by re-running the simulations for the test flights with obstacles under the refined mixed guidance law, having set the initial deviation angle at $\delta_0 = 0$ (i.e., having directed take-off toward the lure, despite the presence of an obstacle blocking the way). These simulations with $\delta_0 = 0$ often produced a collision with the first obstacle, even though no collision was produced when δ_0 was set to the value observed (Figure 4). Consequently, the hawks' biased take-off direction was necessary (and typically sufficient) to cause their target pursuit subsystem (Equation 1) to produce a safe path around the first obstacle. This functional conclusion begs the mechanistic question of how the hawks selected this take-off bias, which we address in the next section.

Take-off bias minimizes obstacle clearance at maximum span

Previous research on obstacle avoidance has found that domestic pigeons *Columba livia domestica* target the centers of gaps between obstacles,[1,2] and that Harris' hawks fixate on the edges of obstacles.[26] We therefore hypothesized that the hawks would take off by aiming at either the nearest edge of the obstacle or the midpoint of the gap between the obstacle and the wall. We tested this by calculating the initial error angle, η_0, between the hypothesized take-off aim and the direction of the hawk's flight and compared this to the equivalent error angle for the lure (i.e., the initial deviation angle δ_0).

The median absolute initial error angle was smaller (Figure 3C) when the hawk was assumed to have aimed its take-off at either the obstacle edge (median $|\eta_0|$: 16.6°; 95% CI: 15.0°, 18.6°) or the gap center (median $|\eta_0|$: 16.1°; 95% CI: 14.4°, 17.6°) rather than the lure (median $|\delta_0|$: 21.2°; 95% CI: 19.8°, 23.8°). However, the initial error angle was smaller again if the hawk was assumed to have aimed for a clearance of approximately one wing length (0.5 m) from the obstacle edge (median $|\eta_0|$: 8.3°; 95% CI: 6.2°, 10.7°), with the median absolute error angle, $|\tilde{\eta}|$, reaching a global minimum of 5° assuming a targeted clearance of 0.6 m on approach to the first obstacle (Figures 5A and 5C). This makes sense because aiming at the edge of an obstacle leaves no clearance, while aiming at the center of a gap leaves more clearance than is necessary for a gap larger than the bird's wingspan. We conclude that the hawks biased

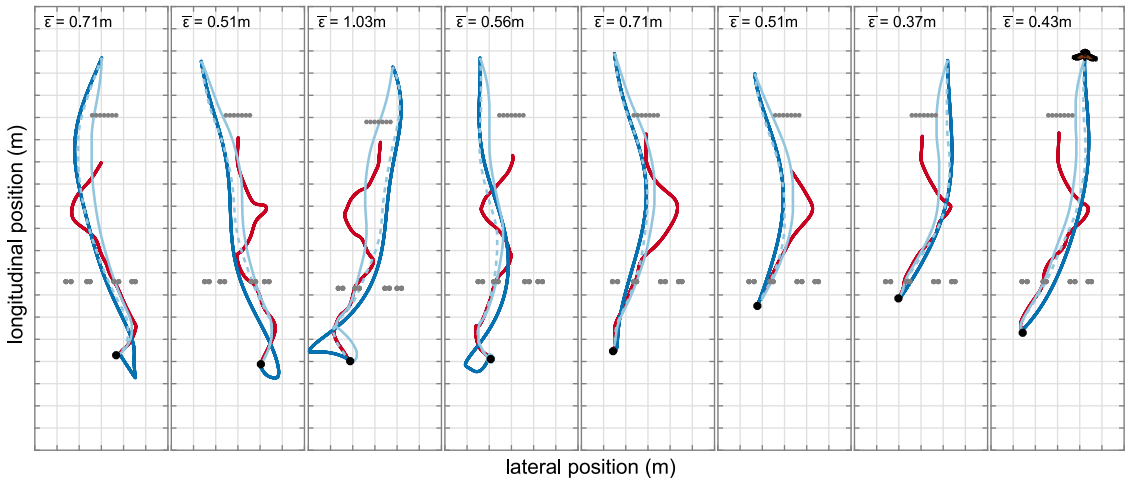

Figure 4. Effect of bias in take-off direction on guidance simulations under the refined mixed guidance law

Each panel represents a single obstacle test flight and plots the hawk's measured flight trajectory (dark blue) in pursuit of the lure (dark red) up to the point of capture (black dot). The measured data are compared to simulations of the hawk's trajectory (light blue) under the refined mixed guidance law (Equation 1), with best-fitting parameters $N = 0.75$, $K = 1.25\ s^{-1}$, and $\tau = 0.01$ s, and (1) the initial deviation angle, δ_0, matched to the value we had measured (dashed line) (2) with the initial deviation angle, δ_0, set so that $\delta_0 = 0$ (solid line), where the displayed values of $\bar{\varepsilon}$ show the mean prediction error for the simulation with $\delta_0 = 0$. Hanging rope obstacles are plotted as gray dots. The lefthand panels show the four longest flights; the righthand panels show the four flights with the lowest mean prediction error relative to the total distance flown, for flights >9 m in length. Grid spacing: 1 m.

their take-off direction to turn tightly around the obstacle without having to close their wings, thereby reconciling any conflict between obstacle avoidance and target pursuit without limiting their control authority. This result is consistent with the theoretical expectation that a bird's minimum turn radius increases in proportion to its wing loading and is therefore minimal at maximal span.[27]

Mid-course steering corrections minimize obstacle clearance at maximum span

The hawks' initial bias in take-off direction explains how they avoided colliding with the first obstacle while chasing the target, but not how they avoided colliding with the second (Figure 3). We therefore looked for evidence of mid-course steering correction by comparing the time history of the median prediction error $\tilde{\varepsilon}(t)$ under the refined mixed guidance law for the n = 154 test flights with obstacles and the n = 103 test flights without (Figure 6).

Because the initial conditions of each simulation were matched to those we had measured, $\tilde{\varepsilon}(0) = 0$ by definition. Thereafter, the simulations deviate from the measured trajectories but do so to a greater extent when obstacles are present (Figure 6). This difference is consistent with our supposition that the hawks made mid-course steering corrections for obstacle avoidance that the simulations under Equation 1 do not capture. Moreover, the median prediction error $\tilde{\varepsilon}(t)$ peaks when the hawks passed the first and second obstacles but does not peak then for the test flights without obstacles (Figure 6). The hawks therefore deviated most from the trajectory commanded by their target pursuit subsystem as they negotiated the obstacles, providing clear evidence of mid-course steering correction using some form of visual look-ahead.[15]

The mechanism of biasing take-off direction that we have identified above provides a prior model of how target pursuit may be combined with obstacle avoidance later in the flight (see also work on obstacle avoidance in human walking behavior[18,19,21]). Specifically, we hypothesize that mid-course steering correction will likewise involve aiming flight for a clearance of approximately one wing length from any obstacle blocking the path to the target. To test this hypothesis, we repeated the error angle analysis that we had undertaken for the first obstacle (Figures 5A and 5C), computing how the error angle, η, varied on approach to the second obstacle in relation to the bird's assumed steering aim (Figures 5B and 5D). Consistent with the results for the first obstacle (Figures 5A and 5C), we found that the median absolute error angle, $|\tilde{\eta}|$, reached a global minimum of 3° when the hawks were assumed to aim for a clearance of 0.65 m from the obstacle (Figures 5B and 5D). This minimum was reached 4 m from the second row of obstacles (Figure 5B), so the hawks appear to have made a mid-course steering correction by the time they were within 4 m of the second obstacle.

Closed-loop versus open-loop steering correction

Avoiding obstacles by aiming flight at a clearance lends itself well to reactive open-loop steering correction, which is the simplest mechanism by which the intermittent demands of obstacle avoidance may be combined with the continuous demands of target pursuit. Under this hypothesis, a one-off steering correction would be made at some threshold distance (or time to collision) from an upcoming obstacle, perturbing the pursuer's deviation angle δ so that the continuation of its pursuit begins with the pursuer heading for a clearance of approximately one wing length from the near edge of the obstacle. This is comparable to an approach used in high-speed autonomous obstacle avoidance,[15] wherein obstacles are first detected at a certain distance using pushbroom stereo, a safe open-loop trajectory is then selected from among a library of possible flight maneuvers, and the chosen maneuver is ultimately executed under

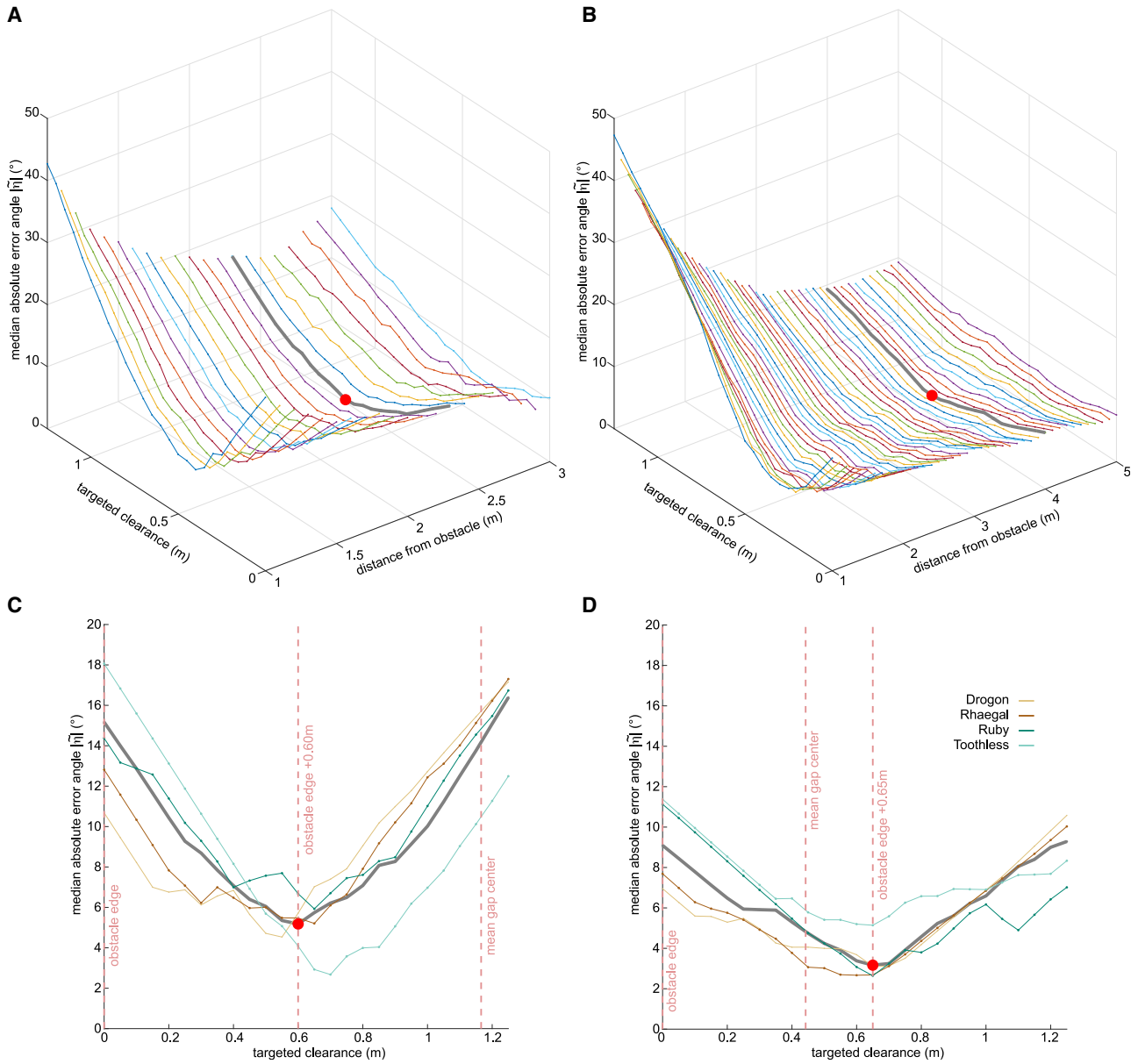

Figure 5. Error angle as a function of targeted clearance from obstacle edge

Plots of the median absolute error angle, $|\tilde{\eta}|$, where the error angle η is defined as the angle between the hawk's flight direction and its line of sight to the clearance, conditional upon the clearance being targeted. Data are shown for the subset of n = 111 obstacle test flights on which the hawk intercepted the target after passing the second obstacle.

(A and B) Median absolute error angle $|\tilde{\eta}|$ as a function of targeted clearance from (A) the first obstacle and (B) the second obstacle, plotted at a range of different distances from the obstacle. The global minimum (red dot) is reached at 2.2 m from the first obstacle (gray line), shortly after take-off, and at 4.0 m from the second obstacle (thick gray line).

(C and D) Median absolute error angle $|\tilde{\eta}|$ as a function of targeted clearance from (C) the first obstacle and (D) the second obstacle, plotted for the specific distance at which the global minimum is reached (thick gray line). The colored lines plot the same quantities for the subset of flights from each individual bird. Red dashed lines denote the locations of the targeted clearances referred to in the main text; note that the exact position of the gap center varies between trials owing to variation in the placement of the obstacles and is therefore summarized by its mean position across trials.

closed-loop control using a linear quadratic regulator.[15] Hence, when we refer to a steering correction as being made in open loop, we refer specifically to the generation of the guidance command—the execution of which could be realized using feedback or feedforward control.

In contrast, previous studies of obstacle avoidance in pigeons[1,2] have modeled steering through clearances as being implemented using a guidance command generated in closed loop, where the gap between obstacles is treated as the goal toward which the bird steers under a guidance law such as

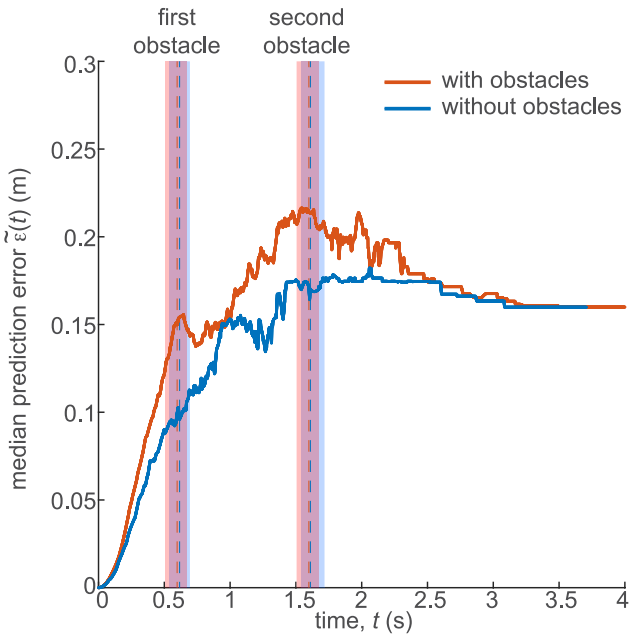

Figure 6. Median prediction error of the refined mixed guidance law against time

Median prediction error $\tilde{\varepsilon}(t)$ between the measured flight trajectories and those simulated under the refined mixed guidance law (Equation 1), with best-fitting parameters $N = 0.75$, $K = 1.25\,s^{-1}$, and $\tau = 0.01$ s. Because the initial conditions of each simulation were matched to those we had measured, $\tilde{\varepsilon}(0) = 0$ by definition. The simulations deviate from the measured trajectories over time but do so to a greater extent on the n = 154 obstacle test flights (orange) than on the n = 103 obstacle-free test flights (blue). The dashed lines and vertical bars denote the median and interquartile range, respectively, of the times at which the hawks passed the locations of the first and second obstacles. Note that the median prediction error peaks at these times for the test flights with obstacles (orange), but not for the test flights without obstacles (blue), providing evidence of mid-course steering correction to avoid them.

Equation 1. Superposing the resulting guidance command with that of a target pursuit subsystem[19] would therefore result in a composite steering command that would represent a continuous compromise between target pursuit and obstacle avoidance, as is also the case in models of human walking behavior.[18,19,21] Hence, provided that the tuning of the guidance parameters is similar for both the target pursuit and obstacle avoidance subsystems, this composite steering command can be modeled by redefining the target of Equation 1 as the point midway between the lure and the gap, which causes no increase in the number of free parameters in the model.

To test for evidence of closed-loop steering correction, we refitted the parameters of the mixed guidance law to the subset of n = 111 obstacle test flights on which the hawk intercepted the target after passing the second obstacle, redefining the target of Equation 1 as the point midway between the lure and a clearance of 0.6 m from the near edge of the second obstacle. For comparison, we also fitted the simulations treating either the lure or the assumed clearance from the obstacle as the target of Equation 1. As before, we matched the initial conditions of the simulations to those we had measured. In each case, we only fitted the simulations as far as the second row of obstacles to avoid the need to redefine the target at this point. We found that the prediction error was smallest for the simulations treating the lure as the target ($\tilde{\varepsilon} = 0.13$ m; 95% CI: 0.12, 0.16 m), largest for the simulations treating the assumed 0.6 m clearance as the target ($\tilde{\varepsilon} = 0.21$ m; 95% CI: 0.20, 0.26 m), and intermediate for the model targeting the point midway between them ($\tilde{\varepsilon} = 0.17$ m; 95% CI: 0.16, 0.19 m). This analysis therefore provides no evidence of closed-loop steering toward the gap between the obstacles, although it does not exclude the possibility that some other mechanism of closed-loop obstacle avoidance may have been in operation.

We therefore tested the alternative hypothesis that Harris' hawks pursue targets through clutter under the mixed guidance law identified above, but that they avoid upcoming obstacles by applying an open-loop steering correction. To model this behavior, we (1) inherited the parameters of the refined mixed guidance law that we had fitted already (i.e., $N = 0.75$, $K = 1.25\,s^{-1}$, and $\tau = 0.01$ s); (2) prescribed the initial conditions by aiming take-off for a clearance of 0.6 m from the near edge of the first obstacle; and (3) added a discrete change in flight direction 4 m ahead of the second obstacle, aiming this for a clearance of 0.6 m from the near edge of the obstacle closest to the hawk's flight direction. In cases where the obstacles were spaced less than 1.2 m apart, such that aiming for a clearance of 0.6 m from one would have brought the bird closer than 0.6 m to the other, we aimed this change in flight direction at the center of the gap between them. We used this model to simulate the subset of n = 111 obstacle test flights on which the hawk intercepted the target after passing the second obstacle (Figure 7) and found that it fitted these data marginally better ($\tilde{\varepsilon} = 0.18$ m; CI: 0.14, 0.22 m) than the refined mixed guidance law with initial conditions matched to those we had measured ($\tilde{\varepsilon} = 0.20$ m; CI: 0.15, 0.25 m). Hence, under the error-free conditions of our simulations, our model of open-loop steering correction is sufficient both to capture the data and to enable successful obstacle avoidance during pursuit under the mixed guidance law.

Target overshoot

Our simulations do not capture every detail of the hawks' turning behavior. For example, the longest test-flight trajectories that we recorded ended with the hawk overshooting the lure, then making a hairpin turn to catch it. This behavior was not captured by the refined mixed guidance law alone (Figure 4), but perturbing the trajectory commanded by the target pursuit subsystem by adding an open-loop steering correction to avoid the second obstacle often caused the simulations to overshoot the lure in a lifelike manner (Figure 7). The fact that a similar overshoot was observed on the test flights without obstacles (Figure S1B) may therefore suggest that the real birds were either unable to generate an accurate steering command (e.g., because of sensor error) or unable to meet this steering demand (e.g., because of physical constraint). It is also possible that this overshoot was adaptive, reflecting an aspect of the control of the final strike maneuver that our guidance simulations do not capture.

Collision risk

Although the rope obstacles that we used were safe by design, collisions with hard obstacles such as tree trunks could be life threatening in the natural environment. Our sample of N = 4 birds is insufficient to draw robust conclusions regarding

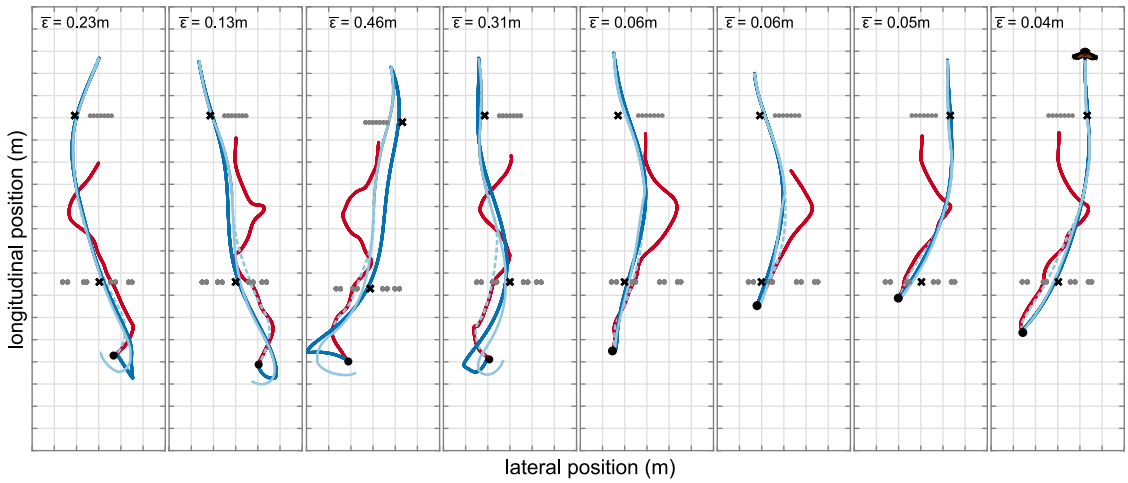

Figure 7. Measured pursuit trajectories of Harris' hawks compared to guidance simulations under the refined mixed guidance law with open-loop steering correction to avoid obstacles

Each panel represents a single obstacle test flight and plots the hawk's measured flight trajectory (dark blue) in pursuit of the lure (dark red) up to the point of capture (black dot). The measured data are compared to simulations of the hawk's trajectory (light blue) under the refined mixed guidance law (Equation 1), with best-fitting parameters $N = 0.75$, $K = 1.25\ s^{-1}$, and $\tau = 0.010$ s, assuming discrete application of a deviation angle bias targeting a clearance of 0.6 m from the nearest edge of an upcoming obstacle (black cross), applied once at take-off in respect of the first obstacle and once at a distance of 4.0 m from the second obstacle. In cases where the gap between obstacles was <1.2 m, this mid-course steering correction was assumed to target the center of the gap, instead of the usual clearance of 0.6 m from the nearest obstacle. The displayed values of $\bar{\varepsilon}$ show the mean prediction error for the corresponding simulation. The dashed line plots the continuation of the simulation without the second steering correction applied to show the effect of its application on obstacle avoidance. Hanging rope obstacles are plotted as gray dots. The lefthand panels show the four longest flights; the righthand panels show the four flights with the lowest mean prediction error relative to the total distance flown, for flights >9 m in length. Grid spacing: 1 m. See also Figure S1.

individual variation in collision risk ($\chi^2(3) = 5.68$; n = 154; p = 0.13), but our subjective impression is that any such variation is mainly attributable to variation in risk aversion rather than flight ability. Overall, we observed collisions occurring on 18% of the n = 154 obstacle test flights (95% CI: 13%, 25%), typically involving clipping of an obstacle by the wing tip feathers, which would be unlikely to cause harm under natural conditions, given the compliant nature of the wings. The birds' observed collision risk was marginally lower, at 13% (95% CI: 6%, 22%), for the subset of n = 72 flights in which the hawk intercepted its target after flying through a gap in the second row of obstacles that was wider than its wingspan. This is comparable to the modeled collision risk of 14% per flight (95% CI: 8%, 24%) predicted by our open-loop model of obstacle avoidance for the same subset, although the modeled collision risk is defined more stringently to include only head-on collisions (STAR Methods).

DISCUSSION

Although it is possible that other guidance laws[28] might explain our hawks' pursuit behavior as well as or better than the mixed guidance law that we have fitted (Equation 1), our modeling demonstrates high repeatability in the guidance parameters fitted across hundreds of flights collected under varying experimental conditions, including different studies on different individuals.[11] Such quantitative repeatability is rare in behavioral studies and presumably reflects both the goal-directed nature of the task and the accuracy of the kinematic measurements that we have used to describe it. In summary, we find that pursuit behavior in Harris' hawks is well modeled by assuming that their turn rate $\dot{\gamma}$ is commanded by feeding back both the angular rate $\dot{\lambda}$ of their line of sight to the target and the deviation angle δ between their flight direction and their line of sight to the target. This closed-loop target pursuit subsystem thereby serves to drive the deviation angle δ to zero, leading to a tail chase that promotes implicit obstacle avoidance if their target follows a safe path through clutter, as was the case on the obstacle familiarization flights (Figure S1A).

In addition, we find that Harris' hawks implement explicit obstacle avoidance (Figure 7) by biasing their take-off direction (Figure 3) and making subsequent mid-course steering corrections (Figure 6) that perturb the deviation angle δ when a collision is imminent (Figure 5). This obstacle avoidance subsystem is well modeled by assuming that the hawks make a discrete steering correction when they encounter an obstacle blocking their path at close range, aiming for a clearance of just over one wing length from its nearest edge. Hence, even when familiar with the obstacle field through which they are flying, Harris' hawks resolve the conflict between obstacle avoidance and prey pursuit by applying a reactive, open-loop steering correction that modifies their closed-loop targeting response in a discontinuous fashion. This avoids the need for forward path-planning, which would be unlikely to be successful when chasing a target whose future trajectory is unknown.

Formally, we have evidence for the following model of obstructed pursuit in Harris' hawks, where turning is commanded at an angular velocity:

$$\dot{\gamma}(t) = N\dot{\lambda}(t-\tau) - K\delta(t-\tau) + \begin{cases} b & \text{if } d \le c_1 \text{ and } \kappa|\eta| \le c_2 \\ 0 & \text{otherwise} \end{cases}, \quad \text{(Equation 2)}$$

where b is a bias command, d is the distance to an upcoming obstacle, and η is the signed angle between the pursuer's flight direction and its line of sight to the near edge of the obstacle. Here $N = 0.75$, $K = 1.25\ s^{-1}$, and $\tau = 0.01$ s are fitted parameters, while $c_1 = 4$ m and $c_2 = \sin^{-1}(0.6/d)$ define the threshold distance and angle at which obstacle avoidance is triggered. The variable κ takes the value $\kappa = -1$ if the pursuer is on a direct collision course with the obstacle, with $\kappa = 1$ otherwise, such that c_2 defines the angular tolerance with which obstacles are avoided. Our specific implementation of Equation 2 in Figure 7 assumes that the bias command is applied as a one-off open-loop steering correction, made over a short time step of duration Δt, such that $b = \mathrm{sgn}\eta(c_2 - \kappa|\eta|)/\Delta t$, where $\mathrm{sgn}\eta$ denotes the sign of the angle η and $|\eta|$ denotes its magnitude at the moment the steering correction is applied. In cases where this steering correction would bring the pursuer's flight direction within the angular tolerance c_2 of another obstacle, the bias command is modified to target the midpoint of the gap between them. This discontinuous, open-loop implementation (see also Barry et al.[15]) has a clear behavioral interpretation, in that the bird is assumed to avoid obstacles by making a saccadic flight maneuver analogous to those observed in insects. Repeated applications of a discrete bias command at distances $d \leq c_1$ from the obstacle would produce a form of closed-loop control, but in our implementation here (Figure 7), the bias command is applied only once in respect of each row of obstacles, thereby justifying its description as an open-loop steering correction.

It is reasonable to suppose that a similar model might successfully describe obstructed pursuit in insects, given the saccadic nature of their flight maneuvers, but previous work on obstructed pursuit in robber flies *Holcocephala fusca* has instead modeled obstacle avoidance as a closed-loop response,[16] with smooth turning commanded as:

$$\dot{\gamma}(t) = N\dot{\lambda}(t-\tau) + \begin{cases} b(t) & \text{if } \dot{\varphi} > 0 \text{ and } |\eta - \delta| \leq c_3 \\ 0 & \text{otherwise} \end{cases}, \quad \text{(Equation 3)}$$

where $\dot{\varphi}$ is the looming rate of a narrow object (i.e., the rate of change in its apparent angular width). Here, $N = 3.6$ and $\tau = 0.03$ s are fitted parameters, while $c_3 = 43°$ is the half-width of the region of interest about the target within which looming objects are treated as obstacles. Although this is still a discontinuous model of obstacle avoidance in the sense that the bias command b is only engaged under certain conditions, steering around obstacles is implemented in closed loop with $b(t) = 0.22\dot{\varphi}(t-\tau_b)\mathrm{sgn}\eta(t-\tau_b)$ at $\tau_b = 0.09$ s, rather than through selection of a new flight direction in open loop (see also Barry et al.[15]). Hence, because the looming rate $\dot{\varphi}$ of an object increases exponentially on approach, so too will the bias command b, except insofar as it causes the pursuer to turn away from the obstacle. Equation 3 has some clear disadvantages, in that it would be complex to implement for a dense obstacle field like the one used in our experiments and commands avoidance of objects that may not necessarily pose a collision risk. It would therefore be of interest to test whether the simpler open-loop model of obstacle avoidance that we have proposed (Equation 2) can successfully model obstructed pursuit in insects.

How might the mid-course steering correction that we have modeled for Harris' hawks be implemented physiologically? The bias command b in Equation 2 is applied at a distance $d \leq c_1$ from an upcoming obstacle, although it is possible that avoidance might be triggered by a bird estimating its equivalent time to collision using optic flow cues.[29] Either way, applying a saccadic steering correction at a fixed distance of $c_1 = 4$ m (or equivalent time to collision) from an upcoming obstacle fixes the angular tolerance for initiating obstacle avoidance at $c_2 = 9°$, simplifying estimation of the angular amplitude $b\Delta t$ of the required steering correction accordingly. This angular tolerance of 9° falls well within the binocular overlap of a Harris' hawk,[30] so it is plausible that a hawk might utilize something analogous to pushbroom stereo[15] to detect obstacles at a given range—even if lacking true stereo vision.[31] Estimation of the angle η between the pursuer's flight direction and the obstacle's edge can be done straightforwardly with reference to the optic flow field if gaze is stabilized rotationally, as occurs during the intervals between head saccades in most birds. In this case, the pursuer's flight direction coincides with the center of expansion of the resulting optic flow field, so the angle η is equal to the angle between the center of expansion and the near edge of the obstacle. The threshold condition $\kappa|\eta| \leq 9°$ (Equation 2) is then met whenever the singularity appears either directly on the obstacle ($\kappa = -1$) or on the background ($\kappa = 1$) within 9° of the edge of the obstacle.

In practice, most visually guided pursuers track their target by turning their head, which complicates the interpretation of the optic flow field by combining rotational and translational self-motion components. However, in an ideal tail-chase, the pursuer's flight direction becomes aligned with the line of sight to its target as the deviation angle δ is driven toward zero. Hence, another simple heuristic, applicable only in a tail-chase, is to approximate the angle η as the difference in azimuth between the target and the near edge of the obstacle. Moreover, a recent pilot study[26] of Harris' hawk gaze strategy during obstructed pursuit found that the bird fixated its target at an azimuth of ±10° with respect to the sagittal plane of its head, coinciding with the assumed projection of its left or right temporal fovea. If this anecdotal result generalizes, such that targets are fixated at ±10° on the right (left) temporal fovea when turning to the right (left) around an obstacle, then at the threshold distance of $d = 4$ m, the steering correction $b\Delta t = 9° - \kappa|\eta|$ that Equation 2 demands would be approximately the azimuth of the obstacle's edge with respect to the head's sagittal plane. Equivalently, if the pursuer's gaze were shifted to fixate the obstacle's edge in the head's sagittal plane, as has also been observed in birds[32] including Harris' hawks,[26] then the amplitude of the required body saccade would be approximately the same as the amplitude of the required head saccade.

The model of obstructed pursuit that we have identified for Harris' hawks is closely related to a form of guidance law from missile engineering called biased proportional navigation.[33] This is a modification of the basic proportional navigation guidance law $\dot{\gamma} = N\dot{\lambda}$ with a bias command b added such that $\dot{\gamma} = N\dot{\lambda} + b$. This is often expressed in the alternative form $\dot{\gamma} = N(\dot{\lambda} - \dot{\lambda}_b)$, by making the substitution $\dot{\lambda}_b = -b/N$. Typically, the bias command b is used to modify the agent's underlying targeting response so as to accomplish some other objective, such as optimizing the control efficiency of a rocket,[33] causing a missile to attain a required impact angle,[34] guiding an autonomous

vehicle along a specified path,[35] or meeting specific rendezvous conditions in spaceflight.[36] Many different variants of biased proportional navigation have been proposed, with bias commands that may be engaged in either a continuous or discontinuous fashion, and that may be specified in either open or closed loop.[37] Our modeling demonstrates another possible technical application of biased proportional navigation (or its generalization to biased mixed guidance), where the bias command is used to implement obstacle avoidance in conjunction with target pursuit.

Our approach to deconflicting obstacle avoidance and target pursuit takes a closed-loop guidance law, such as proportional navigation[5,6] or the mixed guidance law[11,28] of Equation 1, and biases this by applying a discrete open-loop steering command at—and if necessary within (Equation 2)—some threshold distance from an upcoming obstacle. It thereby combines previously unconnected approaches from missile guidance[33–35] and robotics.[15] In so doing, it differs fundamentally from previous studies that have used proportional navigation to model gap negotiation in birds[2] and autonomous vehicles,[38] which treat the clearance beside an obstacle as a virtual target for the guidance law itself. Our approach also differs from related work on human walking behaviors[18,19] in which a single target serving as an attractor and a set of obstacles serving as repellers together produce a smooth turning potential.[21] This contrasts with the saccadic turning behavior resulting from the discontinuous influence of obstacles in our model (see also Barry et al.[15]). Moreover, although these reactive models of human walking behavior superficially resemble the mixed guidance law that we have fitted, insofar as they command steering in proportion to the deviation angle δ and line-of-sight rate $\dot{\lambda}$ of the target,[39] it is the angular acceleration $\ddot{\gamma}$, rather than the angular velocity $\dot{\gamma}$, that is set proportional to δ and $\dot{\lambda}$ in these models.[18,19,21,39] It may therefore be worthwhile to explore whether a model of the form we have fitted here might also explain human walking behaviors.

To conclude, biased guidance offers a biologically inspired mechanism for resolving the conflict between obstacle avoidance and target pursuit, which could be deployed in drones designed to intercept other drones in clutter. Since the same guidance laws can likewise be used to steer flight toward stationary targets, application of an open-loop bias command could also be used for obstacle avoidance during homing flight, or when flying between waypoints.

STAR★METHODS

Detailed methods are provided in the online version of this paper and include the following:

- KEY RESOURCES TABLE
- RESOURCE AVAILABILITY
  - Lead contact
  - Materials availability
  - Data and code availability
- EXPERIMENTAL MODEL AND SUBJECT DETAILS
- METHOD DETAILS
  - Experimental design
  - Experimental protocol
- QUANTIFICATION AND STATISTICAL ANALYSIS
  - Trajectory reconstruction
  - Guidance simulations
  - Parameter estimation

SUPPLEMENTAL INFORMATION

Supplemental information can be found online at https://doi.org/10.1016/j.cub.2023.06.047.

ACKNOWLEDGMENTS

We thank our falconers Mark Parker, Helen Sanders, and Lucy Larkman for their involvement in the experiments, and our mechanical workshop technician John Hogg for designing and building the equipment. We thank James Shelton and Natalia Pérez-Campanero Antolín for helpful conversations. This project has received funding from the European Research Council (ERC) under the European Union's Horizon 2020 research and innovation program (grant agreement no. 682501). J.A.K. was supported by a Christopher Welch Scholarship from the University of Oxford. L.A.F. and S.M. were supported by funding from the Biotechnology and Biological Sciences Research Council (BBSRC) (grant number BB/M011224/1), via the Interdisciplinary Bioscience Doctoral Training Partnership. For the purpose of open access, the author has applied a CC-BY public copyright license to any Author Accepted Manuscript (AAM) version arising from this submission.

AUTHOR CONTRIBUTIONS

Conceptualization, C.H.B., J.A.K., and G.K.T.; formal analysis, C.H.B., J.A.K., L.A.F., M.K.H., S.M., and G.K.T.; methodology, C.H.B., J.A.K., and G.K.T.; investigation, C.H.B., J.A.K., M.K.H., and S.M.; visualization, C.H.B.; supervision, G.K.T.; writing – original draft, C.H.B.; writing – review & editing, G.K.T. All authors reviewed and commented on the original draft.

DECLARATION OF INTERESTS

The authors declare no competing interests.

Received: April 14, 2023
Revised: June 16, 2023
Accepted: June 19, 2023
Published: July 7, 2023

REFERENCES

1. Lin, H.T., Ros, I.G., and Biewener, A.A. (2014). Through the eyes of a bird: modelling visually guided obstacle flight. J. R. Soc. Interface *11*, 20140239. https://doi.org/10.1098/rsif.2014.0239.
2. Antolin, N.P.-C., and Taylor, G.K. (2022). Gap selection and steering during obstacle avoidance in pigeons. J. Exp. Biol. *226*, jeb244215. https://doi.org/10.1242/jeb.244215.
3. Chin, D.D., and Lentink, D. (2022). Birds both avoid and control collisions by harnessing visually guided force vectoring. J. R. Soc. Interface *19*, 20210947. https://doi.org/10.1098/rsif.2021.0947.
4. Ros, I.G., Bhagavatula, P.S., Lin, H.-T., and Biewener, A.A. (2017). Rules to fly by: pigeons navigating horizontal obstacles limit steering by selecting gaps most aligned to their flight direction. Interface Focus *7*, 20160093. https://doi.org/10.1098/rsfs.2016.0093.
5. Brighton, C.H., Thomas, A.L.R., and Taylor, G.K. (2017). Terminal attack trajectories of peregrine falcons are described by the proportional navigation guidance law of missiles. Proc. Natl. Acad. Sci. USA *114*, 13495–13500. https://doi.org/10.1073/pnas.1714532114.
6. Brighton, C.H., Chapman, K.E., Fox, N.C., and Taylor, G.K. (2021). Attack behaviour in naive gyrfalcons is modelled by the same guidance law as in peregrine falcons, but at a lower guidance gain. J. Exp. Biol. *224*, jeb238493. https://doi.org/10.1242/jeb.238493.

7. Kane, S.A., and Zamani, M. (2014). Falcons pursue prey using visual motion cues: new perspectives from animal-borne cameras. J. Exp. Biol. *217*, 225–234. https://doi.org/10.1242/jeb.092403.
8. Mischiati, M., Lin, H.T., Herold, P., Imler, E., Olberg, R., and Leonardo, A. (2015). Internal models direct dragonfly interception steering. Nature *517*, 333–338. https://doi.org/10.1038/nature14045.
9. Fabian, S.T., Sumner, M.E., Wardill, T.J., and Gonzalez-Bellido, P.T. (2022). Avoiding obstacles while intercepting a moving target: a miniature fly's solution. J. Exp. Biol. *225*, jeb243568. https://doi.org/10.1242/jeb.243568.
10. Kane, S.A., Fulton, A.H., and Rosenthal, L.J. (2015). When hawks attack: animal-borne video studies of goshawk pursuit and prey-evasion strategies. J. Exp. Biol. *218*, 212–222. https://doi.org/10.1242/jeb.108597.
11. Brighton, C.H., and Taylor, G.K. (2019). Hawks steer attacks using a guidance system tuned for close pursuit of erratically manoeuvring targets. Nat. Commun. *10*, 2462. https://doi.org/10.1038/s41467-019-10454-z.
12. Surlykke, A., Ghose, K., and Moss, C.F. (2009). Acoustic scanning of natural scenes by echolocation in the big brown bat, Eptesicus fuscus. J. Exp. Biol. *212*, 1011–1020. https://doi.org/10.1242/jeb.024620.
13. Mohta, K., Watterson, M., Mulgaonkar, Y., Liu, S., Qu, C., Makineni, A., Saulnier, K., Sun, K., Zhu, A., Delmerico, J., et al. (2018). Fast, autonomous flight in GPS-denied and cluttered environments. J. Field Robot. *35*, 101–120. https://doi.org/10.1002/rob.21774.
14. Rafai, A.N.A., Adzhar, N., and Jaini, N.I. (2022). A review on path planning and obstacle avoidance algorithms for autonomous mobile robots. J. Robot. *2022*, 2538220. https://doi.org/10.1155/2022/2538220.
15. Barry, A.J., Florence, P.R., and Tedrake, R. (2017). High-speed autonomous obstacle avoidance with pushbroom stereo. J. Field Robot. *35*, 52–68. https://doi.org/10.1002/rob.21741.
16. Fabian, S.T., Sumner, M.E., Wardill, T.J., and Gonzalez-Bellido, P.T. (2022). Avoiding obstacles while intercepting a moving target: a miniature fly's solution. J. Exp. Biol. *225*, jeb243568, https://doi.org/10.1242/jeb.243568.
17. Schöner, G., Dose, M., and Engels, C. (1995). Dynamics of behavior: theory and applications for autonomous robot architectures. Robot. Autonom. Syst. *16*, 213–245. https://doi.org/10.1016/0921-8890(95)00049-6.
18. Fajen, B.R., Warren, W.H., Temizer, S., and Kaelbling, L.P. (2003). A dynamical model of visually-guided steering, obstacle avoidance, and route selection. Int. J. Comput. Vis. *54*, 13–34. https://doi.org/10.1023/A:1023701300169.
19. Cohen, J.A., Bruggeman, H., and Warren, W.H. (2010). Combining moving targets and moving obstacles in a locomotion model. J. Vis. *6*, 135. https://doi.org/10.1167/6.6.135.
20. Rushton, S.K., and Allison, R.S. (2013). Biologically-inspired heuristics for human-like walking trajectories toward targets and around obstacles. Displays *34*, 105–113. https://doi.org/10.1016/j.displa.2012.10.006.
21. Huang, W.H., Hung, P.K., Fink, J.R., and Warren, W.H. (2006). Visual navigation and obstacle avoidance using a steering potential function. Laryngoscope *116*, 288–291. https://doi.org/10.1016/j.robot.2005.11.004.
22. Horiuchi, T.K. (2009). A spike-latency model for sonar-based navigation in obstacle fields. IEEE Trans. Circuits Syst. I. *56*, 2393–2401. https://doi.org/10.1109/tcsi.2009.2015597.
23. Wen, C., and Horiuchi, T.K. (2022). The curved openspace algorithm and a spike-latency model for sonar-based obstacle avoidance. Front. Neurorobot. *16*, 850013, https://doi.org/10.3389/fnbot.2022.850013.
24. Jaksic, F.M., and Carothers, J.H. (1985). Ecological, morphological, and bioenergetic correlates of hunting mode in hawks and owls. Ornis Scand. *16*, 165–172. https://doi.org/10.2307/3676627.
25. Paul, N., and Ghose, D. (2023). Longitudinal-acceleration-based guidance law for maneuvering targets inspired by hawk's attack strategy. J. Guid. Control Dynam. *46*, 1437–1447. https://doi.org/10.2514/1.G007276.
26. Miñano, S., Golodetz, S., Cavallari, T., and Taylor, G.K. (2023). Through hawks' eyes: synthetically reconstructing the visual field of a bird in flight. Int. J. Comput. Vis. *131*, 1497–1531.
27. Taylor, G., and Thomas, A. (2014). Evolutionary Biomechanics (Oxford University Press). https://doi.org/10.1093/acprof:oso/9780198566373.001.0001.
28. Kempton, J.A., Brighton, C.H., France, L.A., KleinHeerenbrink, M., Miñano, S., Shelton, J., and Taylor, G.K. (2023). Visual versus visual-inertial guidance in hawks pursuing terrestrial targets. J. R. Soc. Interface *20*, 20230071, https://doi.org/10.1098/rsif.2023.0071.
29. Wang, Y., and Frost, B.J. (1992). Time to collision is signalled by neurons in the nucleus rotundus of pigeons. Nature *356*, 236–238. https://doi.org/10.1038/356236a0.
30. Potier, S., Bonadonna, F., Kelber, A., Martin, G.R., Isard, P.-F., Dulaurent, T., and Duriez, O. (2016). Visual abilities in two raptors with different ecology. J. Exp. Biol. *219*, 2639–2649. https://doi.org/10.1242/jeb.142083.
31. Martin, G.R. (2009). What is binocular vision for? A birds' eye view. J. Vis. *9*, 14.1–1419. https://doi.org/10.1167/9.11.14.
32. Kress, D., van Bokhorst, E., and Lentink, D. (2015). How lovebirds maneuver rapidly using super-fast head saccades and image feature stabilization. PLoS One *10*, e0129287, https://doi.org/10.1371/journal.pone.0129287.
33. Murtaugh, S.A., and Criel, H.E. (1966). Fundamentals of proportional navigation. IEEE Spectr. *3*, 75–85. https://doi.org/10.1109/MSPEC.1966.5217080.
34. Byung Soo, K., Jang Gyu, L., and Hyung Seok, H. (1998). Biased PNG law for impact with angular constraint. IEEE Trans. Aerosp. Electron. Syst. *34*, 277–288. https://doi.org/10.1109/7.640285.
35. Erer, K.S., Tekin, R., and Özgören, M.K. (2016). Biased proportional navigation with exponentially decaying error for impact angle control and path following, pp. 238–243.
36. Su, W., Yao, D., Li, K., and Chen, L. (2016). A novel biased proportional navigation guidance law for close approach phase. Chinese J. Aeronaut. *29*, 228–237. https://doi.org/10.1016/j.cja.2015.12.014.
37. Erer, K.S. (2015). Biased proportional navigation guidance for impact angle control with extension to three-dimensional engagements. PhD thesis (Middle East Technical University).
38. Han, S.-C., Bang, H., and Yoo, C.-S. (2009). Proportional navigation-based collision avoidance for UAVs. Int. J. Control Autom. Syst. *7*, 553–565. https://doi.org/10.1007/s12555-009-0407-1.
39. Fajen, B.R., and Warren, W.H. (2007). Behavioral dynamics of intercepting a moving target. Exp. Brain Res. *180*, 303–319. https://doi.org/10.1007/s00221-007-0859-6.
40. Potier, S., Mitkus, M., and Kelber, A. (2018). High resolution of colour vision, but low contrast sensitivity in a diurnal raptor. Proc. Biol. Sci. *285*, 20181036, https://doi.org/10.1098/rspb.2018.1036.
41. KleinHeerenbrink, M., France, L.A., Brighton, C.H., and Taylor, G.K. (2022). Optimization of avian perching manoeuvres. Nature *607*, 91–96. https://doi.org/10.1038/s41586-022-04861-4.

STAR★METHODS

KEY RESOURCES TABLE

REAGENT or RESOURCE	SOURCE	IDENTIFIER
Deposited data		
Reconstructed position and trajectory data.	This paper	https://doi.org/10.6084/m9.figshare.21905211
Experimental models: Organisms/strains		
Parabuteo unicinctus	Captive-bred	N/A
Software and algorithms		
Nexus	Vicon Motion Systems Ltd, Oxford, UK	https://www.vicon.com/software/nexus/
MATLAB	Mathworks, MA, USA	https://www.mathworks.com/products/matlab.html
MATLAB code for trajectory reconstructions	This paper	https://doi.org/10.6084/m9.figshare.21905211
MATLAB code for guidance simulations	Brighton and Taylor[11]	https://doi.org/10.1038/s41467-019-10454-z
MATLAB code for parameter estimation	This paper	https://doi.org/10.6084/m9.figshare.21905211

RESOURCE AVAILABILITY

Lead contact

Further information and requests for resources should be directed to and will be fulfilled by the lead contact, Graham Taylor (graham.taylor@biology.ox.ac.uk).

Materials availability

This study did not generate new materials.

Data and code availability

- The reconstructed position and trajectory data has been deposited at figshare and is publicly available as of the date of publication. DOIs are listed in the key resources table. The raw motion capture data will be shared by the lead contact upon request.
- All original code has been deposited at figshare and is publicly available as of the date of publication. DOIs are listed in the key resources table.
- Any additional information required to reanalyze the data reported in this paper is available from the lead contact upon request.

EXPERIMENTAL MODEL AND SUBJECT DETAILS

We used a population of N = 4 captive-bred Harris' hawks *Parabuteo unicinctus* for this study, comprising one experienced 7-year old female (Ruby) that had been included in a previous study of pursuit,[11] and three first-year males (Drogon, Rhaegal, Toothless) that had not previously pursued a target (see Table S1).

The birds were housed individually at the John Krebs Field Station, Wytham, Oxford, UK in open-fronted aviaries separated by a double mesh wall that enabled the birds to see each other and to interact socially without risk of physical contact. The birds were kept tethered during the experimental period, according to conventional falconry practice, and were free lofted at other times. The shelf perch to which each bird was tethered was heated for their comfort during the winter months. The birds were flown 5 days per week during the experiments and were fed a daily ration of wholefood (i.e., day-old chick, quail, mouse) assessed to maintain individual body weight at a level that meant they were motivated to chase the target. The birds' wholefood diet was supplemented with beef during experiments.

This work was approved by the Animal Welfare and Ethical Review Board of the Department of Zoology, University of Oxford, in accordance with University policy on the use of protected animals for scientific research, permit no. APA/1/5/ZOO/NASPA, and was considered not to pose any significant risk of causing pain, suffering, damage or lasting harm to the animals.

METHOD DETAILS

Experimental design

We recorded the flight trajectories of the hawks as they pursued a food lure towed along a zigzagging course around a set of pulleys, with or without obstacles present (Figure 1A). A subset of the flights without obstacles that we report are described and analyzed using a related method elsewhere,[28] but the flights with obstacles are reported here for the first time. Each bird usually flew after the lure four times per day, taking off spontaneously from the falconer's gloved fist when the lure began moving. The lure was hidden inside a tunnel at the start of each test, mimicking a terrestrial prey item being flushed from cover. The lure vanished into another tunnel if the bird failed to catch it by the end of the course, which motivated the birds to catch the lure whilst it was still moving.

The experiments began with an 8-day training phase to familiarize the hawks with the task of chasing the lure without obstacles. This yielded a set of n = 128 obstacle-free training flights (Table S1), following which we introduced obstacles into the environment. We conducted a single day of obstacle familiarization flights, using an open layout comprising two rows of four ropes. This yielded a set of n = 16 obstacle familiarization flights (Table S1) during which the lure was pulled through the gaps between the obstacles. We used a different obstacle arrangement for the main test flights: the first row of test obstacles comprised an impenetrable grille of eight ropes centered on the midline of the flight hall (Figure 1B); the second row of test obstacles comprised four pairs of ropes blocking each of the lure's four possible paths on its way to the last set of pulleys (Figure 1A). This yielded a total of n = 103 obstacle-free test flights and n = 154 obstacle test flights (Table S1), recorded over 15 days of trials including 7 days with obstacles, 5 days without obstacles, and 3 days at the start of the period in which the presence or absence of obstacles was randomized between flights.

We used a simplified pulley configuration at the start of the initial training phase, with four pulleys placed in a diamond-shaped configuration (Pulleys 1-4 in Figure 1A). This layout produced two possible lure courses, with an unpredictable bifurcation at the first pulley followed by two predictable changes in target direction at the next two pulleys. We modified the pulley setup before the end of the training phase, placing six pulleys in a chevron-shaped configuration (Figures 1A and 1B). This layout produced six possible courses, with two or three unpredictable bifurcations in target direction, and one predictable change in direction at the last pulley. The lure course and hawk starting position were randomly assigned before each flight, and we laid dummy towlines to make it harder for the hawks to anticipate the lure's course (Figures 1A and 1B). The speed of the lure was randomized within the range 6-8 m s^{-1} for each flight; at higher speeds, the hawks were unable to catch the lure before the end of the course. Following the initial training phase, we randomized the presence or absence of obstacles between test flights. This took considerable time, however, and was an unnecessary source of stress for the birds, so we subsequently randomized the presence or absence of obstacles once at the start of each day.

Experimental protocol

The experiments were carried out at the John Krebs Field Station, Wytham, Oxford, UK between January and March 2018 in a windowless flight hall measuring 20.2 m by 6.1 m, with an eaves-height of 3.8 m. The flight hall was lit by flicker-free LED up-lights providing approximately 1000 lux of diffuse overhead lighting reflected by white fabric sheets hung from the ceiling to mimic overcast morning or evening conditions. The walls of the hall were hung with camouflage netting to provide visual contrast, and small shrubs and trees were placed down the sides of the room to discourage flight outside of the central test area (Figure 1B). The hawks were flown individually from the gloved fist of a falconer positioned in one of three starting positions across the flight hall (Figure 1A). A falconry lure with a small food reward attached was towed around a series of large pulleys by two Aerotech linear actuators rigged with a block and tackle system to increase their output speed (ACT140DL, Aerotech Limited, Hampshire, UK); a drag line pulled along behind the lure smoothed its path around the pulleys (Figure 1A). For the experiments with obstacles, we hung jute ropes (diameter: 0.05 m) from the roof space to the floor to mimic compliant stems or branches, wrapping them in expanded polystyrene pipe insulation to make them safe in case of collision (Figure 1B).

We reconstructed each flight using 20 motion capture cameras recording at 200 Hz (Vantage 16, Vicon Motion Systems Ltd, Oxford, UK), under stroboscopic 850 nm infrared illumination outside the visible spectrum of Harris' hawks.[40] Four high-definition video cameras (Vue, Vicon Motion Systems Ltd, Oxford, UK) recorded synchronized reference video at 120 Hz. The cameras were mounted on a scaffold at a height of 3 m, spaced around the perimeter of the flight hall to maximize coverage (Figures 1A and 1B). The motion capture system was turned on at least an hour before commencement of the flight experiments and was calibrated immediately before the first trial by moving an Active Calibration Wand (Vicon Motion Systems Ltd, Oxford, UK) through the capture volume. The origin and ground plane of the coordinate system were set by placing the calibration wand on the floor in the center of the room. Each bird was fitted with two rigid marker templates (Figure 1C): a backpack template with four 6.4 mm diameter spherical retroreflective markers arranged in an asymmetric pattern, attached to a falconry harness (Trackpack Mounting System, Marshall Radio Telemetry Ltd, Cumbria, UK); and a tail-pack with three 6.4 mm diameter retroreflective markers, attached to a falconry tail mount (Marshall Aluminium Tail Feather Piece, Marshall Radio Telemetry Ltd, Cumbria, UK). The birds also wore retroreflective markers attached directly to the feathers on their head, wings, or tail, but these are not included in the present analysis. Six 6.4 mm diameter retroreflective markers were attached directly to the lure, with three markers on either side in a back-to-back arrangement. Each rope obstacle was fitted with 9.5 mm diameter markers at eye level and floor level.

QUANTIFICATION AND STATISTICAL ANALYSIS

Trajectory reconstruction

The three-dimensional (3D) positions of the bird, lure, and obstacle markers were reconstructed using Nexus software (Vicon Motion Systems Ltd, Oxford, UK), in a coordinate system aligned to the principal axes of the flight laboratory. Previous work had found that the Vicon software was not always able to identify which marker was which between frames, owing to marker occlusion and the small distance between the markers relative to the distance travelled between frames.[41] We therefore used custom-written code in MATLAB (Mathworks, MA, USA) to label the anonymous markers in the rigid templates. Our first step was to identify markers that remained stationary through the trial as being obstacle markers. For the remaining markers, we used their height above the floor to distinguish between markers on the bird and the lure and used a clustering algorithm to distinguish between markers on the backpack and the tail-pack. We used the centroid of the backpack and lure as our initial estimate of their respective positions, treating any frames in which fewer than three markers were detected on the backpack, tail-pack, or lure as missing data.

The initial position estimates for the backpack, tail-pack and lure were contaminated by misidentified markers, which we excluded by removing points falling further than 0.5 m from the smoothed trajectory obtained using a sliding window mean of 0.05 s span. We then repeated this sliding window mean elimination on the raw data with extreme outliers excluded, this time using a distance threshold of 0.075 m. Our next step was to crop the trajectories to begin at the first frame on which both the bird and lure were visible, and to end at the point of intercept defined as the point of minimum distance between the bird and lure. We then used cubic interpolation to fill in any missing data points and fitted a quintic spline to smooth the 3D data, using a tolerance of 0.03 m for the bird and 0.01 m for the lure. Finally, we double-differentiated the spline functions, which we evaluated analytically to estimate the velocity and acceleration of the bird and lure at 20 kHz, resulting in a suitably small integration step size for our simulations.

Guidance simulations

As the birds always flew close to the ground plane, our guidance analysis concerns only the horizontal components of the pursuit. We used the same forward Euler method and MATLAB code described previously[11] to simulate the hawk's horizontal flight trajectory given the measured trajectory of the lure. We modelled the hawk's turning using the mixed guidance law in Equation 1 for a given set of parameter settings N, K, and τ, matching its simulated flight speed to its measured flight speed. In cases where the hawk's simulated trajectory resulted in an earlier intercept than its measured trajectory, we matched the continuation of the simulated trajectory to that of the lure up to the measured point of intercept. By default, we matched the hawk's initial flight direction in the simulations to that which we had measured. However, we also ran versions of the simulations in which we re-initialized the hawk's flight direction at take-off or 4 m from the second obstacle, by directing its flight towards some specified location (see results). We defined the prediction error for each flight, $\varepsilon(t)$, as the distance between the measured and simulated flight trajectories.

Parameter estimation

We optimized the guidance parameters N, K, and τ by minimizing the median of the mean prediction error, $\tilde{\varepsilon}$, over a given subset of flights. We did this using an exhaustive search procedure for values of N and K from 0 to 2 at intervals of 0.05, and for values of τ from 0 to 0.09 s in intervals of 0.005 s. To ensure that we modelled the same section of flight for all values of τ, we began each simulation at 0.09 s after the start of the trajectory. Although we optimized the guidance parameters for the obstacle and obstacle-free test flights separately at first, we subsequently combined these subsets, owing to the observed similarity of their best-fitting parameter settings. Because there were more test flights with obstacles than without, we used a balanced subsampling procedure to avoid biasing the fitting of the joint model in favor of obstructed pursuit. Specifically, we sampled 80 flights at random from each subset and identified the parameter settings that minimized $\tilde{\varepsilon}$ over that sample. We repeated this sampling experiment 100,000 times and took the grand median of the resulting best-fitting parameter settings as our refined model. We quantified the goodness of fit of a given guidance model by computing the mean prediction error, $\bar{\varepsilon}$, for each flight. We then used a bias corrected and accelerated percentile method to compute a bootstrapped 95% confidence interval for the median of the mean prediction error $\tilde{\varepsilon}$ at the best-fitting parameter settings. We report bootstrapped 95% confidence intervals for other properties of the simulated flight trajectories where relevant, and Agresti-Coull 95% confidence intervals for the observed and modelled collision risk. We calculated the observed collision risk by using the video data to count the proportion of flights in which any part of the bird contacted either row of obstacles, and calculated the modelled collision risk by counting the proportion of flights in which the point corresponding to the bird's center of mass crossed the perimeter of any obstacle.